# Ka-Band Meander-line Slow Wave Structure Design for Traveling Wave Tube for High Data Rate Wireless Links

Mohit Kumar Joshi, Vincent Da Costa, Muhammad Zubair, Ahsan Altaf *Member, IEEE*, Rosa Letizia *Senior member, IEEE*, and Claudio Paoloni, *Senior member, IEEE*

***Abstract*— Ka-band (26 - 40 GHz) is widely used for satellite links. In particular, the 26.5 - 29.5 GHz band is mostly used for uplink in Low Earth Orbit (LEO) constellations and is also part of the FR2 (24.25 GHz to 52.6 GHz) for high capacity terrestrial links. The addition of the 26.5 - 29.5 GHz band for downlink would increase the satellite throughput, but presently SSPA power modules do not provide enough power and have too low efficiency. Ka-band traveling wave tubes (TWTs) are traditionally used in GEO satellite for their high transmission power and high efficiency. Compact and affordable Ka-band TWTs would be a promising solution to provide transmission power to enable downlink at Ka-band. Meander lines (ML) have been extensively investigated as slow wave structures (SWS) for light weight, small dimensions and low voltage operation. In this paper, an interaction circuit for compact and affordable Ka-Band TWTs based on the Meander Line (ML-TWT) is discussed. The first TWT with two meander line sections interacting with an elliptical sheet beam with 4.56 kV beam voltage, in the 26.5 GHz - 29.5 GHz frequency range, is proposed. More than 31 Watt output power with about 38 dB gain in the linear region is achieved. A single-section ML-SWS and a sever for the two-section ML-TWT are fabricated and measured. The compact dimensions and low-voltage of the novel Meander Line TWT (ML-TWT) make it a competitive solution for medium transmission power in future Ka-band high-capacity LEO satellite and terrestrial links for future 5G and 6G network integration.**

***Index Terms*— Ka-band, low-voltage, meander-line (ML), millimeter wave, planar slow-wave structure (SWS), sheet-beam, thermal analysis, traveling-wave tube (TWT), 5G NR.**

## I. Introduction

Non Terrestrial Networks (NTN) are growing of importance in the 5G and 6G global communication scenario by the integration with terrestrial networks for ubiquitous coverage [1]. The Ka-band (26 – 40 GHz) is extensively used for satellite communications in both geostationary (GEO) and LEO (Low Earth Orbit) constellations [2]. LEO constellations use the Ka-band mostly for uplink due to the higher attenuation than the lower frequency Ku-band, typically used for downlink. [3], [4].

Presently, solid-state power amplifiers (SSPAs), typically in GaN or GaAs technology, are used for LEO satellites downlinks able to satisfy the link budget related to the proximity to the Earth and for their large volume availability. Output power up to 80 W is reported by combining multiple chips in the same module [5], [6], but it is not space qualified. Power Added Efficiency (PAE) up to 40 % is reported for saturated output power below 10 W. However, at the increase of the output power and the back-off, the PAE reduces substantially [6]. To note that SSPAs require a complex and bulky cooling system.

Traveling wave tubes (TWTs) are widely adopted for Ka-band downlinks in GEO satellites or scientific space missions. TWTs are particularly suitable for space communication thanks to efficiency better than 50 % and hundred watts of output power, necessary for GEO links. The advantages of TWTs in comparison to SSPAs are low-current, higher efficiency, and high power. TWTs do not need a complex cooling system, since the thermal effects are localized in the collector with a suitable size to effectively dissipate heat. On the contrary, the major thermal effects in SSPAs are localized in the small junction region [7] making difficult to extract the heating. Presently, SSPAs are used in LEO constellations. TWTs would enable high Signal-To-Noise Ratio (SNR), high efficiency links but to be competitive against SSPAs should be more affordable with compact dimensions including the Electronic Power Conditioner (EPC).

The available Ka-band TWTs are mostly based on helix [8] or folded waveguide slow-wave structures (FW-SWSs). Helices ensure a very wide band, but the small diameter required at Ka-band makes them expensive to build. The folded waveguide usually operates at a beam voltage higher than 10 kV and requires a high-accuracy alignment to avoid possible stop-band in-band. Meander line SWSs (ML-SWSs) have been extensively investigated and are very promising slow structures for the medium output power TWTs for satellite links as replacement of SSPAs [9]. ML-SWSs are easy and affordable to fabricate in large volume, have very compact dimensions and are able to support a low beam voltage, e.g., 4 – 5 kV, suitable for a compact and lightweight power supply. Different shapes of ML-SWSs such as U-shaped [10], V-shaped [11], [12], S-shaped [13], omega-shaped [14], rhombus-shaped [15], log-periodic [16] SWSs at different frequencies up to W-band [17]–[20] are reported in the literature. Typically, ML-SWSs support a sheet electron beam. Sheet electron beams require more complex magnetic focusing system than cylindrical electron beam, but permit to have a higher current with lower current density. In this paper a novel two-section ML-SWS for a Ka-band TWT in the 26.5 – 29.5 GHz frequency band is proposed to provide about 30 W saturated output power for high-capacity wireless links both for space and terrestrial application. The TWT shows a gain better than 30 dB with 4.56 kV beam voltage and 100 mA beam current.

The design of the ML-SWS interaction circuit is discussed in Section II. The final topology of a two-section ML-SWS for a Ka-band TWT and particle-in-cell (PIC) simulations are described in Section III. Fabrication and measurement of a single section ML-SWS as simulation validation are discussed in Section IV.

## II. Design of low-voltage Meander Line SWS circuit

The substantial advantage of a meander line SWS in comparison to metal SWSs, such as the folded waveguide, is the shorter period and the support of low beam voltage. At the Ka-band, the ML-SWS period is hundreds of microns against one or two millimeters of metal SWSs, permitting to produce shorter and more compact TWTs.

### A. Cold parameters design

A conventional topology of meander line (Fig. 1) made by Alumina substrate with a copper metal strip was chosen for the SWS design.

This work has been supported by Huawei Technologies Sweden AB. The authors would like to acknowledge the High-End Computing (HEC) at Lancaster University, Lancaster, U.K. for providing access to HEC facility to carry out simulations.

Mohit Kumar Joshi, Vincent Da Costa, Muhammad Zubair, Rosa Letizia and Claudio Paoloni are with the School of Engineering, Lancaster University, Lancaster, LA1 4YW, United Kingdom, Ahsan Altaf is with Huawei Technologies, Sweden AB, Sweden

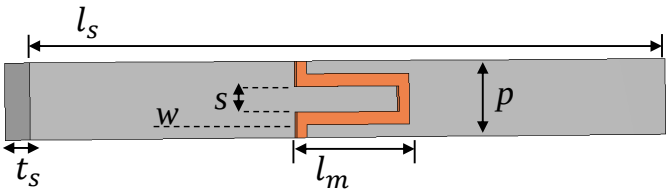


Fig. 1. Unit-cell of the ML-SWS.

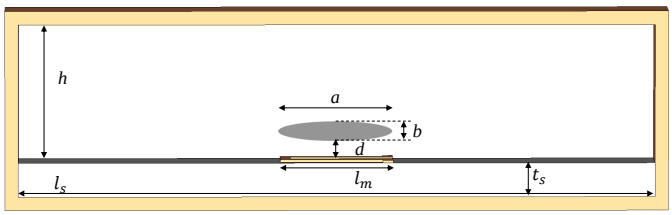


Fig. 2. Cross-section of the ML-SWS with the rectangular waveguide envelope.

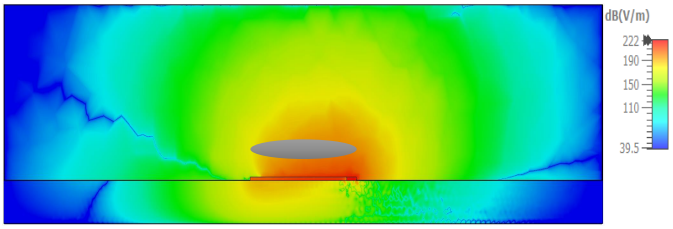


Fig. 3. E-field (axial component) distribution on the ML-SWS cross-section.

No specific advantage was found in the use of different ML-SWS topologies. The unit-cell of the ML-SWS is modeled by CST Studio [21] as depicted in Fig. 1. The metal strip is 30 $\mu$m thick. The copper conductivity is set $\sigma = 4.5 \times 10^7$ S/m to include the attenuation due to the surface roughness of the copper strip. Alumina substrate 96% (dielectric constant $\epsilon_r$ = 9.9 and loss tangent tan$\delta$ < 0.0004), with 250 $\mu$m thickness, is used because of its good thermal properties, relatively low cost and availability on the market, and to be easily cut by laser cutter. The ML-SWS is housed inside a rectangular waveguide in stainless steel as shown in Fig. 2 . An extensive study on the ML properties at slightly higher frequency in the Ka-band range was performed in [19]. On that basis, the optimization of the cold parameters of the ML-SWS, specifically dispersion and interaction impedance, is performed by the eigenmode solver of CST MS [21]. The target is to achieve the synchronism with a beam voltage below 5 kV over the desired 26.5 - 29.5 GHz frequency band. The dimensions of the ML-SWS are listed in Table I. The dimensions of the sheet beam are defined based on the EM-field distribution over the ML-SWS, that in this case corresponds to the width $l_m$= 850 $\mu$m of the unit-cell (Fig. 3). The dispersion curves of the first two modes with a superimposed 4.56 kV beam line are shown in Fig. 4, corresponding to 0.13$c$ phase velocity. The intercept with the second mode is out of the band and can be neglected.

The interaction impedance of the ML-SWS in the operating frequency band computed over the electron beam section is shown in Fig. 5. About 8.5 Ω at the center of the band is obtained, value that ensures good interaction level of the propagating EM-field with the electron beam.

A tolerance sensitivity analysis has been performed on the main design parameters of ML-SWS, such as period ($p$) ($\pm$ 20 $\mu$m) , metal thickness ($t_m$) ($\pm$ 5 $\mu$m), and length ($l_m$). Figure 6 shows that

TABLE I
DIMENSIONS OF THE ML-SWS

| Parameters | Values |
|---|---|
| Substrate width ($l_s$) | 4800 $\mu m$ |
| Substrate thickness ($t_s$) | 250 $\mu m$ |
| Meander-line period ($p$) | 462 $\mu m$ |
| Meander-line length ($l_m$) | 850 $\mu m$ |
| Meander-line thickness ($t_m$) | 20 $\mu m$ |
| Meander-line width ($w$) | 77 $\mu m$ |
| Gap between strips ($s$) | 154 $\mu m$ |
| Waveguide height ($h$) | 1250 $\mu m$ |
| Sheet beam cross section ($a \times b$) | 850 $\mu m$ × 250 $\mu m$ |
| Sheet beam distance from the meander-line ($d$) | 50 $\mu m$ |

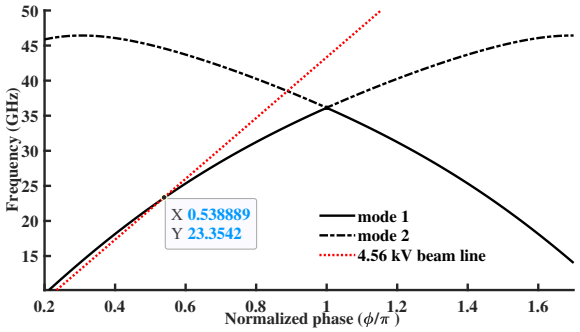


Fig. 4. Dispersion curves of the first two modes of the ML-SWS with 4.56 kV beamline superimposed.

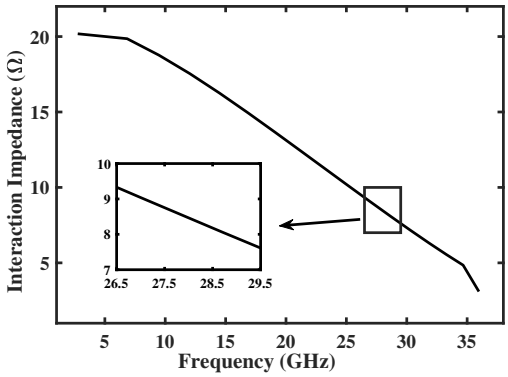


Fig. 5. Interaction impedance of the ML-SWS as a function of the frequency.

the interaction impedance is practically not affected. The normalized phase velocity has a maximum variation of about $\pm$ 5 %, that can be compensated with a variation of the beam voltage. Figure 7 shows the sensitivity of the interaction impedance as a combined function of the period ($p$) for different lengths ($l_m$) of ML-SWS ($\pm$ 10% against the nominal value). The variation in length ($l_m$) has a substantial impact that requires an accurate mask alignment. The normalized phase velocity (Fig. 8) as expected is sensitive to both the parameters ($p$ and $l_m$), in particular more to the length $l_m$. The curves in Fig. 7 and 8 can also be used as design charts for defining the dimensions for a specific value of normalized phase velocity.

### B. ML-SWS Interaction circuit

The interaction circuit includes the ML-SWS with the number of periods to provide a required gain and the transitions to connect the ML-SWS to the input and output ports. The ML-SWS coupler is

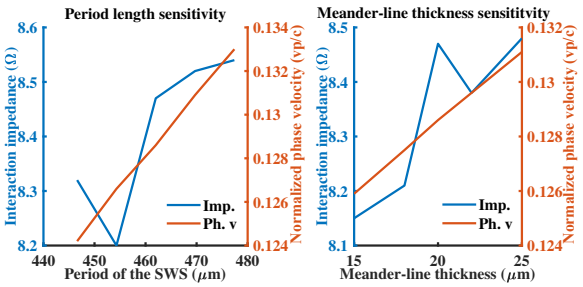


Fig. 6. Sensitivity analysis of interaction impedance and normalized phase velocity of the meander-line as a function of o period ($p$) and thickness ($t_m$).

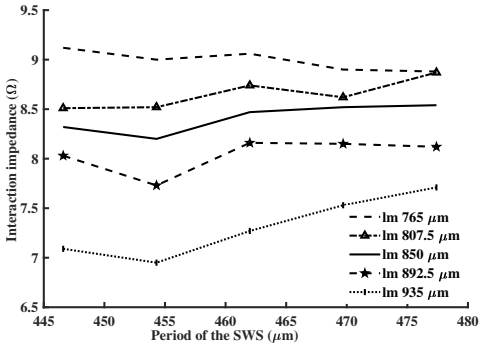


Fig. 7. Sensitivity of the interaction impedance to the period ($p$) and length ($l_m$).

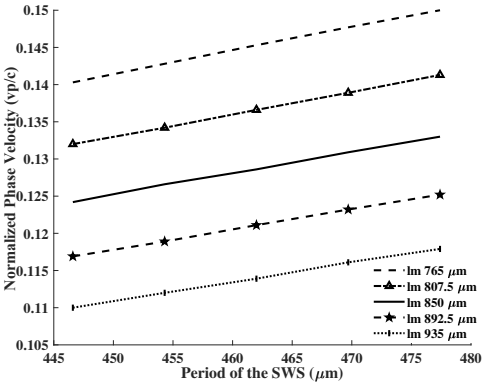


Fig. 8. Sensitivity of the normalized phase velocity to the period ($p$) and length ($l_m$).

a tapered straight microstrip section connected to a 50 Ω microstrip section connected to the coaxial transition for measurement purposes. The interaction circuit is shown in Fig. 9. The couplers are placed at 90° to the meander line to allocate the input and output ports at the side of the TWT. The housing has a U-shaped profile pocket to accommodate the alumina substrate, holes for the bead of the 2.92 mm connectors, and the input and output aperture for the beam tunnel. A 40-period ML-SWS is simulated. The $S$-parameters are shown in Fig. 10. The $S_{11}$ is better than -20 dB in the operation band. The insertion loss is about -5 dB. The described interaction circuit can be considered as the unit section for the design of a multi-section ML-SWS TWT, which is described in the next section.

### C. Sheet beam and permanent periodic magnetic focusing

A sheet electron beam with 4.56 kV beam voltage and 100 mA beam current is adopted. The sheet beam has an elliptical cross-section 850 $\mu m$ wide and 250 $\mu m$ high. The uniform Brillouin

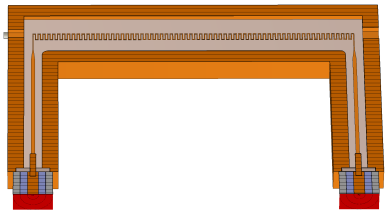

Fig. 9. Single-section ML- SWS with coaxial coupler at the input and output ports.

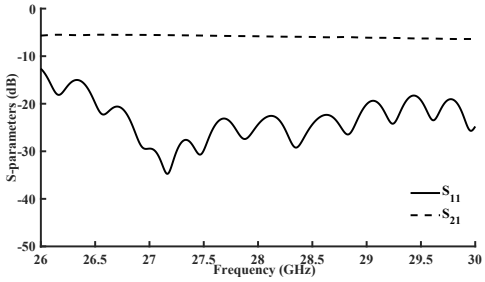


Fig. 10. $S$-parameters of the single-section ML-TWT.

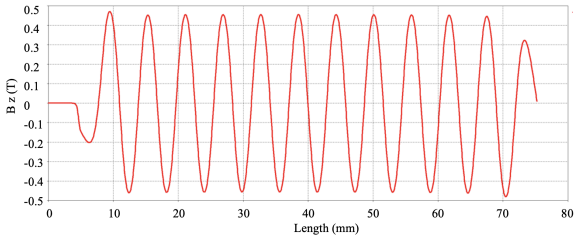


Fig. 11. Magnetic field $B_z$ distribution along the beam tunnel axis

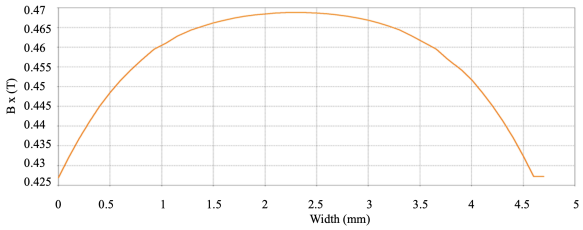


Fig. 12. Magnetic field $B_x$ distribution over the cross-section of the beam tunnel

field ($B_r$) for the electron beam is calculated as 0.139 T. The rms value of the minimum required longitudinal magnetic focusing field ($B_z/\sqrt{2}$) of about $2B_r$ is considered for the beam confinement. A periodic permanent magnetic (PPM) system has been designed for the focusing of the sheet beam. The PPM stack is made by rectangular magnets of Neodymium (NdFeB) with 1.1 T remanence alternated with rectangular soft iron pole pieces. The PPM structure is simple and of easy tuning. A magnetic field of about $B_z$=0.4 T has been obtained, suitable to confine the sheet electron beam in both longitudinal direction and over the cross-section of the sheet beam. Fig. 11 and Fig. 12 show the magnetic field $B_z$ distribution over the length (beam axis) and the magnetic field $B_x$ over the cross-section of the beam tunnel. The PPM provides an excellent sheet electron beam confinement as shown in Figs. 13(a) and 13(b).

## III. Two-section ML-SWS for a Ka-band TWT

The interaction circuit for the ML-SWS TWT (Fig. 14) is designed with two sections with 65 and 80 periods, respectively, to obtain

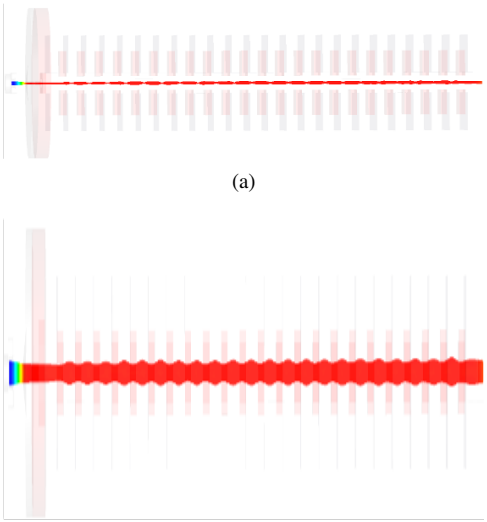

(a)

(b)

Fig. 13. Sheet beam trajectory along the beam tunnel axis. (a) side-view. (b) top-view.

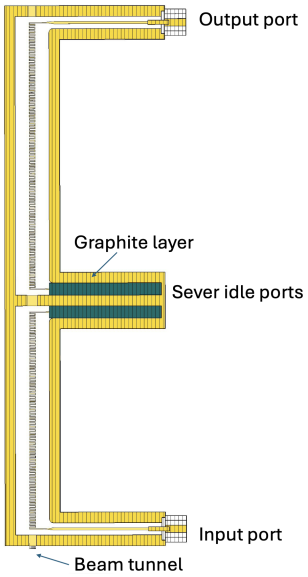


Fig. 14. Two-section ML-SWS interaction circuit with sever

about 30 W output power and a 35 dB gain in the 26.5 - 29.5 GHz frequency band. The first low-gain section provides the beam current modulation. The second section provides the required amplification and output power. A sever isolates the two sections for the RF to avoid oscillations. It comprises two terminated couplers (idle ports) and the beam tunnel as a waveguide under cut-off to RF that isolates the two sections. A graphite sheet is used as an absorber to fill the volume of the termination at the output of the first section and of the termination at the input of the second section. The obtained $S_{11}$ at the input port of the two-section ML-SWS TWT is below -20 dB in the entire frequency band (Fig. 15) indicating the good matching of the sever terminations.

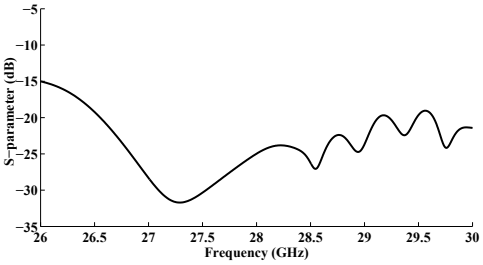


Fig. 15. $S_{11}$ of the input port of the two-section ML-SWS.

## A. Large signal performance

The large signal performance of the two-section ML-SWS interaction circuit is evaluated by using Particle-in-Cell (PIC) simulations (CST-PS) with beam voltage and beam current of 4.56 kV and 100 mA, respectively. An elliptical beam cross-section (850 $\mu m$ major axis and 250 $\mu m$ minor axis) is defined. An input power of 12 mW is applied. A static magnetic field with a value suitable (about two times the PPM $B_z$ field) to provide the same beam focusing as the PPM field in Fig. 11 is used in the PIC simulations. This is due to the different behavior in simulation of the static magnetic field in comparison to a real PPM magnetic field. [22].

The output power ($P_{out}$) and the gain as a function of frequency are plotted in Fig. 16. An output power better than 44 dBm and an average gain of about 33 dB over the 26.5 - 29.5 GHz frequency band are obtained. The maximum output power (32.97 W or 45.18 dBm) in saturation and gain (34.39 dB) are achieved at 28.5 GHz. Fig. 17 shows the RF power along the length of the interaction circuit, calculated at 28.5 GHz. The peaks in the RF power at the position of the couplers are due to a post processing conversion of the quasi-TEM mode of the microstrip line to the hybrid mode of the meander line making the field locally stronger. The output power ($P_{out}$) and the gain as a function of the input power ($P_{in}$) obtained at 28 GHz (center frequency of the desired frequency band) are plotted in Fig. 18. To note the 1-dB compression point at about 44 dBm ( 25 W). A 3 dB backoff corresponds to approximately 41 dBm ($\sim$ 13 W) of output power.

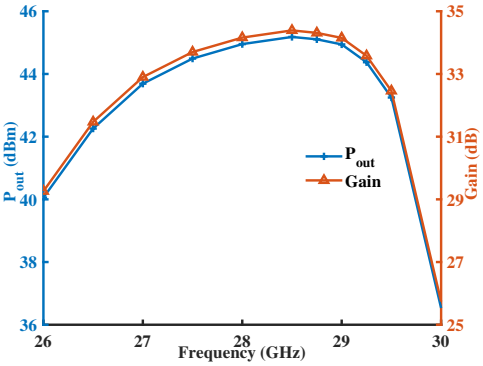


Fig. 16. Output power ($P_{out}$) and gain of two-section ML-SWS as a function of frequency.

## B. Thermal analysis of the ML-SWS

A thermal analysis has been performed by coupled EM-thermal simulation in CST Studio. Particle and EM losses are imported from the PIC simulation into the steady-state thermal solver. Since no particle collision is observed in the PIC simulation, only EM losses affect the temperature distribution profile. The thermal distribution in the ML-SWS at 28.5 GHz is shown in Fig. 19. The ML-SWS is surrounded by air at $25^{\circ}C$ ambient temperature. The thermal emissivity of copper, alumina, and graphite is considered as 0.3, 0.75, and 0.85, respectively. The convective heat transfer coefficient of the outer surface is set to 15 $W/m^2/K$ for natural cooling. The maximum temperature obtained is $111^{\circ}C$ at the end of the second

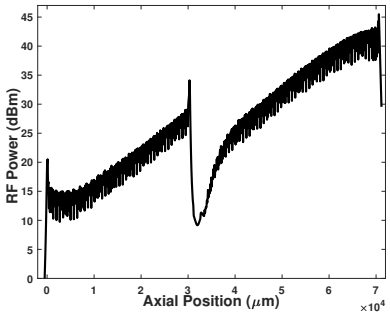


Fig. 17. RF power versus the length of the ML interaction circuit.

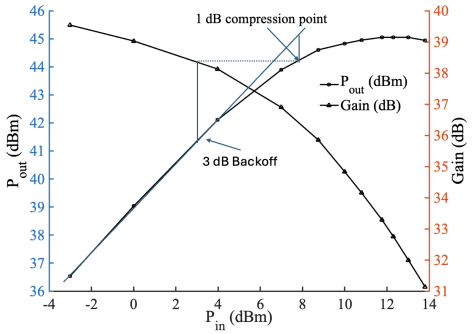


Fig. 18. Output power ($P_{out}$) and gain as a function of input power ($P_{in}$) of two-section ML-SWS at 28.5 GHz.

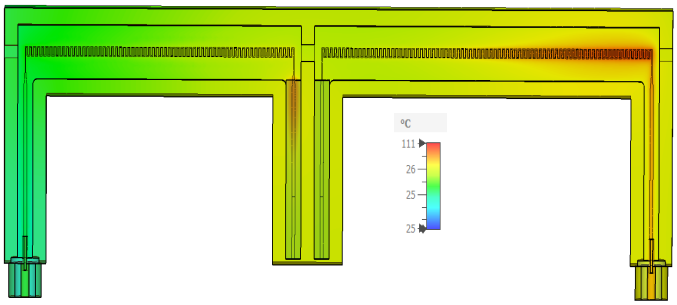


Fig. 19. Steady state temperature distribution of the two-section ML-TWT.

section of TWT, as shown in Fig. 19. The thermal behavior of the ML-SWS interaction circuit does not raise concerns and in space application a radiation-cooled collector will be adopted.

## IV. Measurements of a Single Section ML-SWS

Two different topologies of ML-SWSs have been realized on an alumina substrate with 250 $\mu$m thickness. One is a meander line with straight input and output (S-ML) couplers to verify the quality of the fabrication and the $S$-parameters with a simple configuration as shown in Fig. 20. The second structure has the same topology that will be used for the TWT, a U-shape with the input and output couplers at $90^{\circ}$ to the meander line.

### A. S-parameter measurements

The $S$-parameters of the two ML-SWSs are compared to assess the eventual impact of the bend of the lateral couplers. The S-ML SWS is shown in Fig. 20(a) which is placed in a straight housing for the measurement of $S$-parameters as shown in Fig. 20(b). This measurement setup is closed by a top lid to enclose the ML-SWS in a closed rectangular waveguide. The U-shaped meander line (U-ML)

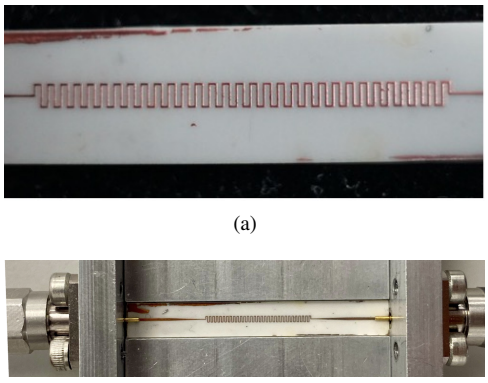

(a)

(b)

Fig. 20. Detail of the straight coupler meander line (S-ML). (a) S-ML slow-wave structure. (b) S-ML with fixture for $S$-parameters measurement.

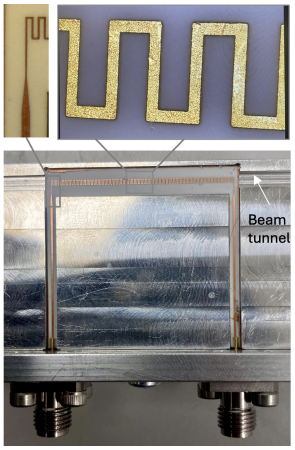


Fig. 21. Housing with U-meander line for $S$-parameter measurement with detail of the meander line.

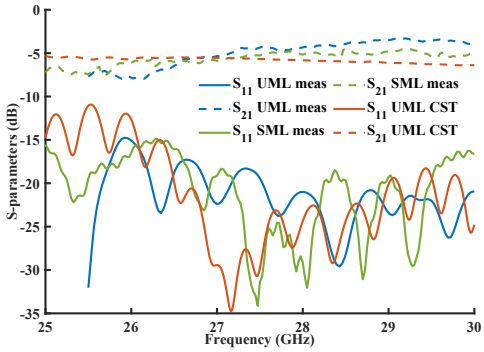


Fig. 22. Comparison of the measured $S$-parameters of the U-ML and S-ML, and simulated $S$-parameters of U-ML.

is measured by a specific fixture as shown in Fig. 21. The fixture is closed by a top lid and also includes the apertures for the beam tunnel.

The measured $S$-parameters ($S_{11}$ and $S_{21}$) of the U-ML and the straight ML (S-ML) are shown in Fig. 22. The $S_{11}$ UML measured at the input port is better than -15 dB, and the measured $S_{21}$ UML is about -5 dB, in agreement with the $S$-parameters ($S_{11}$ UML CST and $S_{21}$ UML CST) obtained from simulation. It is noteworthy the agreement with the simulations and the similar performance of the measured two different coupler ML-SWSs.

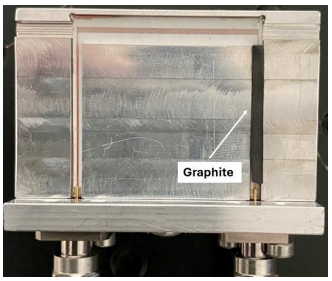


Fig. 23. U-ML with absorption material (graphite) in the output port for sever measurement.

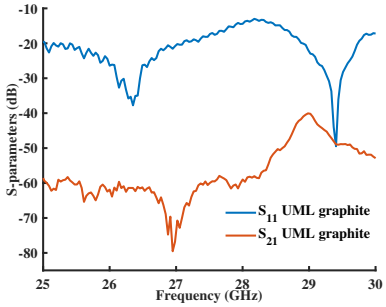


Fig. 24. $S_{11}$ and $S_{21}$ of the U-ML with graphite absorber in Fig. 23.

### B. Sever measurement

The sever has been built and tested. A layer of graphite has been placed on the microstrip line at one of the couplers used as termination port as shown in Fig. 23. Figure 24 shows the measured $S_{11}$ better than -13 dB and the $S_{21}$ lower than -40 dB. The sever provides full absorption of the wave propagating to the idle port. The $S$-parameters of the ML-SWS and the sever performance demonstrates the feasibility of the two-stages interaction circuit in Fig. 14.

## V. Conclusions

A novel two-section Ka-band meander line interaction circuit for a Ka-band TWT is discussed a promising solution for medium-power, high-linearity, and high-efficiency TWTs for high-capacity wireless links at Ka-band for space applications. The small dimensions and the low beam voltage of a ML-TWT make it a competitive alternative to lower power and lower efficiency SSPAs. The ML-SWS has low production cost and is suitable for large volume, with substantial benefits for a widespread adoption of ML-SWS TWTs to enable high capacity links at Ka-band both satellite and terrestrial for network integration and increasing traffic demand for 5G and future 6G. To note that ML-SWS is scalable to higher frequencies. The fabrication of the ML-SWS TWT is in an advanced phase.

## References

[1] X. Lin, S. Rommer, S. Euler, E. A. Yavuz, and R. S. Karlsson, "5G from space: An overview of 3GPP non-terrestrial networks," *IEEE Communications Standards Magazine*, vol. 5, no. 4, pp. 147–153, 2021.

[2] S. Boumard, I. Moilanen, M. Lasanen, T. Suihko, and M. Höyhtyä, "A technical comparison of six satellite systems: Suitability for direct-to-device satellite access," in *2023 IEEE 9th World Forum on Internet of Things (WF-IoT)*, 2023, pp. 01–06.

[3] R. De Gaudenzi, P. Angeletti, D. Petrolati, and E. Re, "Future technologies for very high throughput satellite systems," *International Journal of Satellite Communications and Networking*, vol. 38, no. 2, pp. 141–161, 2020. [Online]. Available: https://onlinelibrary.wiley.com/doi/abs/10.1002/sat.1327

[4] S. Liu, Z. Gao, Y. Wu, D. W. Kwan Ng, X. Gao, K.-K. Wong, S. Chatzinotas, and B. Ottersten, "Leo satellite constellations for 5G and beyond: How will they reshape vertical domains?" *IEEE Communications Magazine*, vol. 59, no. 7, pp. 30–36, 2021.

[5] S. D. Yoon, J. Kitt, D. Murdock, E. Jackson, M. Roberg, G. Hegazi, and P. Courtney, "Highly linear amp; efficient power spatium combiner amplifier with gan hpa mmic at millimeter wavelength frequency," in *2020 IEEE/MTT-S International Microwave Symposium (IMS)*, 2020, pp. 416–419.

[6] H. Wang and *et al.* Power amplifiers performance survey 2000-present. https://ideas.ethz.ch/research/surveys/pa-survey.html. [Online]. Available: https://ideas.ethz.ch/research/surveys/pa-survey.html

[7] E. Illokken, "Twt reliability in space," *IEEE Aerospace and Electronic Systems Magazine*, vol. 2, no. 7, pp. 22–24, 1987.

[8] W. L. Menninger, N. R. Robbins, D. R. Dibb, and D. E. Lewis, "Power flexible ka-band traveling wave tube amplifiers of up to 250-w rf for space communications," *IEEE Transactions on Electron Devices*, vol. 54, no. 2, pp. 181–187, 2007.

[9] J. M. Socuéllamos, R. Dionisio, R. Letizia, and C. Paoloni, "Experimental validation of phase velocity and interaction impedance of meander-line slow-wave structures for space traveling-wave tubes," *IEEE Transactions on Microwave Theory and Techniques*, vol. 69, no. 4, pp. 2148–2154, 2021.

[10] S. Sengele, H. Jiang, J. H. Booske, C. L. Kory, D. W. Van der Weide, and R. L. Ives, "Microfabrication and characterization of a selectively metallized W-band meander-line TWT circuit," *IEEE transactions on electron devices*, vol. 56, no. 5, pp. 730–737, 2009.

[11] F. Shen, Y. Wei, H. Yin, Y. Gong, X. Xu, S. Wang, W. Wang, and J. Feng, "A novel V-shaped microstrip meander-line slow-wave structure for W-band MMPM," *IEEE Transactions on Plasma Science*, vol. 40, no. 2, pp. 463–469, 2011.

[12] S. Wang, S. Aditya, X. Xia, Z. Ali, J. Miao, and Y. Zheng, "Ka-band symmetric V-shaped meander-line slow wave structure," *IEEE Transactions on Plasma Science*, vol. 47, no. 10, pp. 4650–4657, 2019.

[13] N. Bai, L. Gu, C. Shen, J. Feng, F. Liao, and X. Sun, "S-shaped microstrip meander-line slow-wave structure for W-band traveling-wave tube," in *2013 IEEE 14th International Vacuum Electronics Conference (IVEC)*. IEEE, 2013, pp. 1–2.

[14] L. Liao, Y. Wei, L. Lu, L. Yue, T. Tang, W. Wang, and Y. Gong, "A novel omega-shaped microstrip slow-wave structure for 60-GHz traveling-wave tube," in *2013 International Workshop on Microwave and Millimeter Wave Circuits and System Technology*. IEEE, 2013, pp. 328–331.

[15] F. Shen, Y. Wei, X. Xu, J. Lai, M. Huang, G. Zhao, and Y. Gong, "Rhombus-shaped microstrip meander-line slow-wave structure for 140 GHz traveling-wave tube," in *IVEC 2012*. IEEE, 2012, pp. 389–390.

[16] S. Wang, Y. Gong, Y. Hou, Z. Wang, Y. Wei, Z. Duan, and J. Cai, "Study of a log-periodic slow wave structure for Ka-band radial sheet beam traveling wave tube," *IEEE Transactions on Plasma Science*, vol. 41, no. 8, pp. 2277–2282, 2013.

[17] Z. Wang, X. Liu, Q. Hu, Y. Gong, Z. Duan, H. Gong, Z. Lu, S. Wang, and J. Feng, "A ka-band angular log-periodic meander-line sws supported by diamond rods," *IEEE Transactions on Electron Devices*, vol. 69, no. 3, pp. 1374–1379, 2022.

[18] S. Wang, S. Aditya, X. Xia, Z. Ali, and J. Miao, "On-wafer microstrip meander-line slow-wave structure at ka-band," *IEEE Transactions on Electron Devices*, vol. 65, no. 6, pp. 2142–2148, 2018.

[19] J. M. Socuéllamos, R. Letizia, R. Dionisio, and C. Paoloni, "Large signal analysis of a new meander line topology for w-band traveling wave tubes," in *2019 12th UK-Europe-China Workshop on Millimeter Waves and Terahertz Technologies (UCMMT)*, 2019, pp. 1–2.

[20] J. M. Socuéllamos, R. Letizia, R. Dionisio, and C. Paoloni, "Novel meander line slow wave structure for w-band twt," in *2020 45th International Conference on Infrared, Millimeter, and Terahertz Waves (IRMMW-THz)*, 2020, pp. 1–2.

[21] "CST Studio 2024," accessed 2025-1-15. [Online]. Available: https://www.3ds.com/products-services/simulia/products/cst-studio-suite/

[22] D. Zhao, X. Lu, Y. Liang, X. Yang, C. Ruan, and Y. Ding, "Researches on an $x$-band sheet beam klystron," *IEEE Transactions on Electron Devices*, vol. 61, no. 1, pp. 151–158, 2014.